The Cryosphere Discuss., 4, 31–75, 2010
www.the-cryosphere-discuss.net/4/31/2010/

The Cryosphere Discussions

This discussion paper is/has been under review for the journal The Cryosphere (TC). Please refer to the corresponding final paper in TC if available.

Monitoring ice shelf velocities from repeat MODIS and Landsat data – a method study on the Larsen C ice shelf, Antarctic Peninsula, and 10 other ice shelves around Antarctica

T. Haug[1], A. Kääb[1], and P. Skvarca[2]

[1]Department of Geosciences, University of Oslo, P.O. Box 1047 Blindern, 0316 Oslo, Norway
[2]Instituto Antártico Argentino, Cerrito 1248, C1010AAZ Buenos Aires, Argentina

Received: 21 December 2009 – Accepted: 31 December 2009 – Published: 14 January 2010

Correspondence to: T. Haug (torborg.haug@geo.uio.no)

Published by Copernicus Publications on behalf of the European Geosciences Union.

Abstract

We investigate the velocity field of the Larsen C ice shelf, Antarctic Peninsula, over the periods 2002–2006 and 2006–2009 based on repeat optical satellite data. The velocity field of the entire ice shelf is measured using repeat low resolution MODIS data (250 m spatial resolution). The measurements are validated for two ice shelf sections against repeat medium resolution Landsat 7 ETM+ pan data (15 m spatial resolution). Horizontal surface velocities are obtained through image matching in both frequency and spatial domain, and the two methods compared. The uncertainty in the displacement measurements turns out to be less than 70 m for the MODIS derived data, and less than 15 m for the Landsat derived ones. The difference between MODIS and Landsat based speeds is $-15.4\,\mathrm{m\,a^{-1}}$ and $13.0\,\mathrm{m\,a^{-1}}$, respectively, for the first period for the two different validation sections on the ice shelf, and $-26.7\,\mathrm{m\,a^{-1}}$ and $27.9\,\mathrm{m\,a^{-1}}$ for the second period for the same sections. This leads us to conclude that repeat MODIS images are well suited to measure ice shelf velocity fields and monitor their changes over time. The frequency domain image correlation method seems better suited for this purpose because it is faster, produces fewer mismatches, and is able to match images with regular noise and data voids. The latter makes it possible to match Landsat 7 ETM+ images even after the 2003 failure of the Scan Line Corrector (SLC off) that leaves significant image sections with no data. Image matching based on the original 12-bit radiometric resolution MODIS data produced slightly better results than using the 8-bit version of the same images. Streamline interpolation from the obtained surface velocity field on Larsen C indicates ice travel times of up to 450 to 550 a between the inland boundary and the ice shelf edge. In a second step of the study we test our method successfully on 10 other ice shelves around Antarctica demonstrating that the approach presented could in fact be used for large scale monitoring of ice shelf dynamics.

1 Introduction

Velocities of glaciers, ice sheets and ice shelves can be measured successfully by remote sensing techniques. The two most commonly used methods so far have been radar interferometry and correlation of repeat images. Radar interferometry measures the phase shifts between two acquisitions. This relies on phase coherence, and in order to avoid coherence degradation, tandem missions with only a few days between the acquisitions are often required. This limits the application of the radar interferometry method. Image correlation has, in principle, much longer coherence times. These can range from about a year for mountain glaciers to more than ten years for Antarctic glaciers and ice streams. The correlation method can be applied to both optical images and to data from synthetic aperture radar (SAR). Image matching can either be done in the spatial domain or the frequency domain (Brown, 1992; Zitova and Flusser, 2003).

Ice velocity studies using the correlation method have among others been conducted in Antarctica (e.g., Scambos et al., 1992), on Svalbard (e.g., Rolstad et al., 1997; Kääb et al., 2005), in the Alps (e.g., Kääb, 2002; Berthier et al., 2005), in New Zealand (e.g., Kääb, 2002; Quincey and Glasser, 2009), in the Himalaya (e.g., Scherler et al., 2008; Kääb, 2005), and in Patagonia (e.g., Skvarca et al., 2003). However, very few have studied ice shelf velocities using the correlation method. Bindschadler et al. (1994) derived velocities using this method on the relatively small Larsen A Ice Shelf. Skvarca (1994) and Glasser et al. (2009) measured the velocities of a small section of the Larsen C Ice Shelf as part of larger studies.

The purpose of this study is, firstly, to demonstrate that optical sensors with low spatial resolution can be used to measure the velocity fields of Antarctic ice shelves and their changes with satisfactory accuracy. Secondly, the study aims at an initial selection of ice shelves where the method presented could actually be employed for easy and operational monitoring of ice flow. Three major advantages of low resolution optical sensors such as MODIS or MERIS are: (1) that they cover much larger areas with a single image than medium and high resolution optical and SAR sensors such as

Landsat, SPOT, Radarsat, ERS SAR or Envisat ASAR do. This fact allows for large-scale monitoring of ice velocities. In addition, it ensures that one individual scene will in most cases contain stable ground. That helps to accurately co-register the repeat data without having to rely on the satellite-derived geolocation of the data or without having to mosaic scenes that stem from different times and contain only moving targets. (2) The very frequent acquisitions of low resolution satellite imagery of up to several times per day in polar regions increases drastically the potential for cloud-free scenes compared to medium and high resolution optical sensors with much lower repeat times. (3) Coherence over time for optical data is often much more robust than the phase coherence of SAR data necessary for SAR interferometry or speckle tracking, allowing to cover much larger time steps using optical data.

On the other hand, application of repeat low resolution optical images for ice shelf velocity measurements has also clear disadvantages: (1) image matching accuracy is in general governed by the pixel size so that sensors with higher spatial resolution potentially provide better accuracies and signal-to-noise ratios. (2) Phase-based methods such as SAR interferometry and SAR speckle tracking will naturally provide a much higher displacement accuracy than image intensity correlation methods as necessary for optical data. (3) Optical sensors are unable to image during (polar) night and through cloud cover. (4) Matching of repeat optical data relies on optical surface contrast features that are naturally scarce over Antarctica. SAR backscatter features suitable for matching will often be denser.

The above list of potential advantages and disadvantages shows that measuring velocity fields on ice shelves using low resolution optical data will not be the optimal method for such work but rather represent a valuable complement to the other methods, which all have different specific benefits and limitations.

The potential and accuracy of ice shelf velocities from low resolution optical data (here: MODIS) is assessed using repeat optical images of medium spatial resolution (here: Landsat) to validate the measurements based on low resolution data. As detail test site we select the Larsen C ice shelf and the remains of the Larsen B ice shelf, both located on the Antarctic Peninsula (Fig. 1). The velocity measurements are conducted using two image matching methods, normalized cross-correlation operating in the spatial domain and orientation correlation operating in the frequency domain, and these two approaches are compared. Velocities are also measured for different periods in order to identify possible velocity changes.

Ice shelves on the Antarctic Peninsula have experienced a considerable rise in both air and sea temperatures over the last decades. Turner et al. (2005) found that air temperatures on the Antarctic Peninsula rose by 0.56 °C decade^{-1} from 1951 to 2000. Meredith and King (2005) reported that the ocean surface temperatures increased by more than 1 °C in the period 1955 to 1998.

At the same time the ice shelves and glaciers in this area have undergone large changes. As many as seven ice shelves have disintegrated over the last decades (Cook and Vaughan, 2009). Several studies have shown that the glaciers feeding the ice shelves have increased their velocities after the disintegration. This speed up has been attributed to removal of the buttressing ice shelves (Scambos and Bohlander, 2003; De Angelis and Skvarca, 2003; Rignot et al., 2004; Scambos et al., 2004; Rignot et al., 2005). In addition, surge activity has been observed after ice shelf disintegration (De Angelis and Skvarca, 2003). The glaciers on the Antarctic Peninsula have also accelerated because their termini have thinned (Pritchard and Vaughan, 2007). As a result of the velocity increase of glaciers on the Antarctic Peninsula, glaciers in this region were considered to lose 60 ± 46 Gt a^{-1} in 2006, which was an increase of 140% since 1996 (Rignot et al., 2008).

Four ice shelves on the northeastern coast of the Antarctic Peninsula have disintegrated between 1986 and 2002. Larsen Inlet started the disintegration process in 1986 and it ended in 1989 (Skvarca, 1993). The ice shelf in Prince Gustav Channel collapsed between 1992 and 1995 (Rott et al., 1996). Larsen A collapsed in 1995 (Rott et al., 1996), and Larsen B followed in 2002 (Rack and Rott, 2004).

It has been observed that several of the ice shelves that disintegrated underwent large changes before they collapsed. Bindschadler et al. (1994) found that Larsen A accelerated by up to 15% from the period 1975–1986 to the period 1986–1989 while Skvarca et al. (1999) measured on Larsen B an acceleration of 13.2% between the periods 1988–1994 and 1994–1997. Furthermore, field measurements carried out along the center flowline of Larsen B revealed that surface ice-velocity which increased by 10% from 1996–1997 to 1997–1999 has augmented to 26% between 1997–1999 and 1999–2001, i.e. just before the final collapse (Skvarca et al., 2004). On the other hand, Vieli et al. (2006) derived from satellite interferometry a maximum increase in ice velocity on Larsen B of about 150 m a^{-1} from 1995/1996 to 1999. Larsen B also thinned before it collapsed with an average thinning rate of -0.17 ± 0.11 m a^{-1} between 1992 and 2001 (Shepherd et al., 2003). According to the same study also Larsen C thinned with -0.08 ± 0.04 m a^{-1} in the period 1992–2001. The thinning was more pronounced in the north, with some parts in the south actually thickening. Griggs and Bamber (2009) found that most of Larsen C is between 150 and 350 m thick.

It has been widely discussed whether the penetration of meltwater into crevasses is enhancing the fractures and thereby trigging the disintegration (Scambos et al., 2000; MacAyeal et al., 2003; Scambos et al., 2008). However, as Vieli et al. (2006) point out, this can only explain the final collapse and not the dynamic response that can be seen prior to the collapse. Because the ice shelves that have disintegrated so far have shown a dynamic response prior to the collapse, we suggest that studying changes in ice shelf dynamics can give valuable insight on their stability.

After introducing the satellite data used, we describe the image matching methods applied and their accuracy. Then, the results for Larsen C are presented in detail in order to understand the potential and limitations of the method. Results for ten other ice shelves in Antarctica are also described in order to evaluate the applicability and performance of the method for Antarctic ice shelves in general and to present an initial selection of ice shelves that could be monitored that way. Discussion and conclusions terminate our study.

2 Satellite data

Optical satellite images with two different spatial resolutions are selected for this study. NASA's Moderate-resolution Imaging Spectroradiometer (MODIS) images (bands 1 and 2) with a spatial resolution of 250 m represent the lowest spatial resolution, and NASA/USGS' Landsat 7 Enhanced Thematic Mapper Plus (ETM+) panchromatic images (channel 8) with a spatial resolution of 15 m represent the highest. The MODIS images have been preprocessed by the National Snow and Ice Data Center (NSIDC) (Scambos et al., 2009) and downloaded from http://www.nsidc.org/. Landsat images are downloaded from http://glovis.usgs.gov/.

Images from three different times are selected in order to measure both velocities over the two periods and velocity changes between the periods. The periods should be long enough to identify statistically significant displacements, but also short enough to avoid surface changes that hinder the correlation of images. Two areas on Larsen C are chosen to validate the velocities and the velocity changes measured with the MODIS imagery. These areas are hereafter referred to as Larsen C South and Larsen C North. The validation is performed by using the finer spatial resolution imagery from the Landsat ETM+ pan sensor. "Larsen C South" indicates images from path 216 row 108 and "Larsen C North" indicates images from path 216 row 107. Their location is indicated in Fig. 1. The validation areas are selected based on the availability of cloud free images from both the MODIS and the Landsat sensors with as short as possible time separation between both. An overview of the selected images can be found in Table 1.

Until autumn 2005 NSIDC produced images with 8 bit radiometric resolution from the MODIS images. Therefore the MODIS image from 2002 is 8 bit, while the images from 2006, 2008 and 2009 are 12 bit, which is the original radiometric resolution of MODIS. The images from 2006, 2008 and 2009 are also available as 8 bit images, and this gave us also the opportunity to investigate the impact of different radiometric resolutions on image matching.

Due to the small elevation differences on the Larsen ice shelf, there are only minor topographic distortions caused by elevation differences in the images. These are assessed to be small enough to be neglected in this study. The matching can therefore be conducted directly on the georeferenced, but not orthorectified satellite images as provided by NSIDC.

3 Image matching methods

3.1 Normalized cross-correlation

Matching of two images can be done using the image intensities directly in the normalized cross-correlation method (NCC). The first image is taken as the reference image, and a window of this image is searched for in the second image, or the search image. The cross-correlation surface CC is given by

$$\mathrm{CC}(i,j) = \frac{\sum_{k,l}(r(i,j)-\mu_r)(s(i,j)-\mu_s)}{\sqrt{\sum_{i,j}(r(k,l)-\mu_r)^2\sum_{i,j}(s(i,j)-\mu_s)^2}} \quad (1)$$

where (i,j) indicates the position in the search area, (k,l) the position in the reference area, r the pixel value of the reference chip, s the pixel value of the search chip, μ_r the average pixel value of the reference chip and μ_s the average pixel value of the search chip. The peak of the cross-correlation surface indicates the displacement between the images.

This method has been widely used for measuring the displacement of both glaciers and rockglaciers (e.g., Kääb, 2002, 2005; Kaufmann and Ladstädter, 2003; Debella-Gilo and Kääb, 2010).

3.2 Orientation correlation

The second matching method is based on the orientation correlation method (OC), which is developed by Fitch et al. (2002). We conduct the matching in the frequency

TCD
4, 31–75, 2010

domain. Matching in the frequency domain works with the image frequencies instead of working directly with the image intensities. Correlation and convolution are related operations, and convolution in the spatial domain equals multiplication in the Fourier domain (the convolution theorem).

When using OC new orientation images are created from the original images based on the image intensity differences in both the horizontal x direction and in the vertical y direction. Central differences are used, except at the edges where forward and backward differences are used to maintain the image size. Taking f as the image at time $t = 1$ and g as the image at time $t = 2$, the orientation images f_o and g_o are created from

$$f_o(x,y) = \mathrm{sgn}\left(\frac{\partial f(x,y)}{\partial x} + i\frac{\partial f(x,y)}{\partial y}\right) \tag{2}$$

$$g_o(x,y) = \mathrm{sgn}\left(\frac{\partial g(x,y)}{\partial x} + i\frac{\partial g(x,y)}{\partial y}\right) \tag{3}$$

$$\text{where } \mathrm{sgn}(x) = \begin{cases} 0 & \text{if } |x| = 0 \\ \frac{x}{|x|} & \text{otherwise} \end{cases} \tag{4}$$

where sgn is the signum function and i is the complex imaginary unit. The new images f_o and g_o are complex and hence consist of one real and one imaginary part, where the intensity differences in the x direction represent the real matrix and the intensity differences in the y direction represent the imaginary matrix. The orientation images are divided into matching windows before the matching is conducted. Such windows should be small enough to avoid having different displacements inside the same window, but large enough to get a clear correlation maximum. In this study we use matching windows of 44×44 pixels (11 000 m) for the MODIS imagery and 350×350 pixels (5250 m) for the Landsat imagery. The spacing between the matching windows is the same as the size of the windows to give a densely populated grid with non-overlapping, independent measurements. The correlation surface $P(x,y)$ is then computed from

$$P(x,y) = \mathrm{IFFT}\left(\frac{F_o(u,v)G_o^*(u,v)}{|F_o(u,v)G_o^*(u,v)|}\right) \tag{5}$$

where $F_o(u,v)$ is the Fast Fourier Transform (FFT) of the matching window from $f_o(x,y)$, $G_o(u,v)$ is the FFT of the matching window from $g_o(x,y)$, * denotes the complex conjugated and IFFT is the Inverse Fast Fourier Transform. The shift that is needed to register the two matching windows is found from the position of the maximum of the correlation surface.

Subpixel accuracy is obtained following the method of Argyriou and Vlachos (2007). Subpixel displacements in the x direction dx and in the y direction dy are found using

$$dx = \frac{P(x_m+1,y_m)-P(x_m-1,y_m)}{2(2P(x_m,y_m)-P(x_m+1,y_m)-P(x_m-1,y_m)} \tag{6}$$

$$dy = \frac{P(x_m,y_m+1)-P(x_m,y_m-1)}{2(2P(x_m,y_m)-P(x_m,y_m+1)-P(x_m,y_m-1)} \tag{7}$$

where $P(x_m,y_m)$ is the maximum correlation value. This means that a parabolic function is fitted to the maximum point and the two surrounding points. When dividing by the amplitude in Eq. (5), only the phase of the FFT is kept. This makes the correlation peak narrower and hence the subpixel accuracy better.

When matching the Landsat images, the orientation images are filtered in the Fourier domain using a finite impulse response (FIR) filter. This is done to remove the high frequencies, and after this filtering the images can be matched using smaller matching windows than before the filtering is conducted. This implies that the low frequencies contain the displacement information and that the high frequencies represent noise in this particular case.

Fourier domain methods have some constraints. Firstly, displacements larger than half the window size can not be measured directly due to the quadrant ambiguity problem. If larger displacements are expected, the images should be aligned beforehand based on the expected displacement. Secondly, the window sizes have generally to be larger than if the matching is done in the spatial domain.

The clear advantages of frequency domain over spatial domain methods are that they can be fast if FFT is used, and that they are not sensitive to image information which is constrained to few frequencies. In this study that turns out to be particularly useful, because the Landsat 7 ETM+ images from 2003 and onward have regular cross-track data voids, i.e. voids with a very specific frequency (Fig. 2), after a failure of the Scan Line Corrector (SLC).

3.3 Accuracy

To quantify the uncertainty of the matching methods, displacement measurements over stable ground are investigated. The displacement measurements in both x and y direction are searched for trends. Only zeroth order trends (i.e. mean translations) are found to influence our level of accuracy, and these translations are therefore subtracted from the measured displacements. The uncertainty of the matching methods is given by the root mean square error (RMS) of the displacement measurements of stable ground, see Table 2.

The Landsat images over Larsen C North from Table 1 and Fig. 1 cover not enough stable ground to detrend the data. Instead, images from the neighbour path 217 row 106 are used to align the images. These neighbour images are taken on 6 April 2002 and 11 January 2006. They include some of the same grounded, low-velocity ice shelf area as the Larsen C North images. These neighbour images (i.e. path 217 row 106) are first aligned using stable bedrock. Then, the ice velocities over the grounded low-velocity area are found, and these velocities are finally used to align the Larsen C North images applied in this study. Because the mean velocity is $12\,\mathrm{m\,a^{-1}}$ the error arising from assuming identical velocity in 2006–2009 is considered small enough for this use. Matching of another neighbour image pair, 3 February 2006 and 25 December 2008 from path 218 row 107, confirmed the 2006–2008 velocities from Larsen C North with a mean difference of $-1.9\,\mathrm{m\,a^{-1}}$. The uncertainty is considered to be somewhat higher than for the Landsat images with stable ground present in the images, and a maximum uncertainty of 15 m in both x and y direction in both periods is assumed.

Outside the areas with stable ground, the attitude variations (variations in the roll, pitch and yaw) of the satellite may contribute to reduced accuracy. The potential for reduced accuracy can be analyzed based on the characteristics of the sensors. Sensors aboard MODIS and Landsat are whiskbroom sensors that scan pixel by pixel unlike linear array pushbroom sensors. Data from whiskbroom systems are therefore exposed to both along-track and cross-track geometrical distortions due to attitude variations. These errors are not fully accounted for in the RMS of stable ground, because this RMS only comes from limited areas in the images. Wolfe et al. (2002) estimate the geolocation accuracy for MODIS to be 50 m. For Landsat the geolocation accuracy is 250 m and the image-to-image registration accuracy is 7.3 m according to NASA (1996).

In the measured displacements over stable ground and over the ice shelf, obvious matching outliers are removed manually. Because there is displacement variation over the ice shelf, but not over the stable ground, it is possible that somewhat fewer of the mismatches are filtered out over the ice shelf compared to the stable ground. It is therefore possible that the accuracy decreases slightly over the ice shelf. This effect is, however, difficult to quantify.

Mismatches could also be removed automatically using the signal-to-noise ratio (SNR) because correct matches have generally a stronger correlation peak compared to erroneous matches. In this study a threshold of approximately 5 would have removed most of the erroneous matches and left most of the correct matches. However, SNR is not used in this test study because we wanted to have full control over the selection process to not remove any correct matches.

In the following we estimate the total uncertainty of our displacement measurements to be the root sum square (RSS) of (i) the RMS of the matches on stable ground and (ii) the above image-to-image registration accuracy. The RMS from matching over stable ground and the registration accuracy are then assumed to be independent. Since this image-to-image registration accuracy is not known to us for MODIS we use the total geolocation accuracy of 50 m for this sensor instead. That way, our uncertainty estimate for MODIS resembles a worst-case scenario. It is assumed that all the individual displacement matchings are dependent ($n = 1$), which is a second accuracy worst-case scenario.

4 Results for Larsen C

4.1 Orientation correlation

OC produces a densely populated network of correct matches between the MODIS images from 2002 and 2006 (Fig. 3) and in particular between the MODIS images from 2006 and 2009 (Fig. 4). Also the two images from 2002 and 2009, nearly seven years apart, are correctly matched for most of the ice shelf (Fig. 5). The ice flows relatively slowly in the inner parts of the ice shelf and accelerates as it approaches the ice shelf edge to the east, as is to be expected. We found highest velocities for the central to southern outer part of the ice shelf, with velocities of approximately 700 m a^{-1}. The directions of the flow generally fit the crevasse pattern and the visible obstacles.

The displacements derived from MODIS images for the period 2002–2006 and the period 2006–2009 are summed up and compared with displacements directly derived from the MODIS images of 2002 and 2009. Only windows that are correctly matched (from manual inspection) in all three matchings are used for the multitemporal comparison. Over the ice shelf the average displacement difference is −36.3 m with an RMS of 149.6 m ($n = 70$). In the flow direction the average displacement difference is −49.0 m with an RMS of 183.8 m, and in the transverse direction it is 21.5 m with an RMS of 141.4 m. Over stable ground the average displacement difference is 33.5 m and the RMS is 44.9 m. The uncertainty of this comparison, calculated using the RSS of the RMS over stable ground and the image-to-image registration accuracy from literature, is ± 117 m.

Velocity measurements on the Landsat images are mostly restricted to the crevassed areas (Fig. 6 and 7). As for the MODIS-derived data, the flow directions obtained from the repeat Landsat images fit the crevasse pattern and flow obstacles, and the velocity increases as the ice moves off the inland boundary. The sections with the highest measured velocities on the MODIS images are also covered by the Landsat images. The latter images also indicate velocities of approximately 700 m a^{-1} in this area.

When comparing MODIS and Landsat derived velocities, we first select all MODIS points which have velocity measurements from both periods 2002–2006 and 2006–2009. Then we do the same for the Landsat points, and at last we select a subset of the Landsat and MODIS points that are less than 11 km apart (the length of the sides of one MODIS matching window). This results in 6 MODIS points (see blue colored arrows in Fig. 3) in the Larsen C North section and 28 MODIS points (see green colored arrows in Fig. 3) in the Larsen C South section. For every MODIS point the average of the Landsat points that have this MODIS point as their closest neighbour is calculated. The average Landsat and MODIS derived velocity is then compared. In our procedure it is not possible to directly compare Landsat-derived and MODIS-derived displacements on a point-by-point base because we use different window sizes for Landsat and MODIS, and match the Landsat data in their original geometry, i.e. not geocoded, in order to avoid resampling artifacts. The results of the comparison can be seen in Table 3 and the uncertainties of the results in Table 4. Landsat measures higher average velocities than MODIS in the south, and lower average velocities in the north. In the south the velocities were not significantly different in the two periods, but in the north both sensors measured a velocity increase from the first period to the second period. The RMS of the average velocities are highest in the south. This reflects the fact that the southern section covers larger velocity gradients.

A difference in average annual velocity between the periods 2002–2006 and 2006–2009 is evident from the MODIS images also for the remains of Larsen B. The four points measured on this ice shelf reveal a mean speed increase of 135 m a^{-1} with an RMS of 26.3 m a^{-1}. This is an increase of approximately 30%. The uncertainty here is ± 28.3 m a^{-1}. Other velocity changes are not statistically significant from the MODIS measurements.

4.2 Comparison between orientation correlation and normalized cross-correlation

Normalized cross-correlation (NCC) does not produce such a dense velocity field as OC when the matching is conducted in a regular grid using the same window size as used for OC (44×44 pixels). This can be seen if comparing Fig. 4 showing the velocity field created by the OC and Fig. 8 showing the velocity field created by NCC. These two velocity fields are obtained by matching the same images with the same position and size of the matching windows. OC produces 332 correct velocity vectors, whereas NCC produces only 129 correct vectors. The RMS of the NCC measurements over stable ground are similar to the RMS of the OC measurements (27.8 m in the x direction and 29.5 m in the y direction). The mean velocity difference for points on the ice shelf measured using both methods is 19.4± 63.4 m a^{-1} ($n = 75$), OC measuring the higher velocities on average. The mean velocity difference over stable ground is 15.1 ± 6.9 m a^{-1} ($n = 108$), NCC measuring the higher velocities on average. The uncertainty of the OC is ± 21.8 m and the uncertainty of the NCC is ± 21.5 m.

NCC gives correct matches even if the window size is decreased. On the MODIS images, window sizes of 15×15 pixels still give correct matches in areas with good contrast, for example crevassed areas (Fig. 9). However, the RMS of the measurements over stable ground increases quickly, and when a window size of 15×15 pixels is chosen, the RMS is as high as 75 m.

From autumn 2005 and onward, the MODIS images from NSIDC are also available with the original MODIS 12 bit radiometric resolution, in addition to 8 bit that are available for all dates. Both frequency and spatial domain matching methods are therefore tested on images with different radiometric resolution in order to assess differences between using 12 bit images instead of 8 bit images for matching. Matching with OC and a windowsize of 44×44 pixels on the 12 bit images from 5 January 2006 and 28 November 2008 produces 390 correct matches, whereas the 8 bit images produce 346 correct matches using the same matching windows. This means that the 8 bit images produce 11.3% fewer correct matches than the 12 bit images. A total of 7 points are correctly matched using the 8 bit images but not correctly matched using the 12 bit images. Matching with NCC and a windowsize of 15×15 pixels at manually pre-selected points with good visual contrast produces 322 correct matches on the 12 bit images. When the matching is repeated at the exact same locations using the 8 bit images, 24 of these points (7.5%) do not produce correct matches. Vice-versa, matching at manually pre-selected points using NCC on the 8 bit images gives 276 correct matches, and when the matching is repeated at the same locations using the 12 bit images, 11 of the points (4.0%) produce mismatches. The RMS of the measurements over stable ground does not change when the 8 bit images are used instead of the 12 bit images, presumably reflecting the good contrast present over the stable areas.

4.3 Streamlines

Streamlines are hypothetical particle tracks interpolated from a velocity field under the assumption that the velocity field applied does not change over time (Kääb et al., 1998). That is, they do not necessarily resemble real particle trajectories. Comparing computed streamlines to actual cumulative flow features such as longitudinal flowlines or crevasse patterns is an additional accuracy check, but it can also be used to indicate if the assumption of a steady-state velocity field might apply. Lack of coincidence between the streamlines interpolated from the current velocity field with flow features reflecting past or cumulative flow conditions hints to past changes in the flow field. Streamlines can also, under the restriction that they do not resemble real particle trajectories, be used for surface age estimates.

Here, streamlines are calculated from the 2006–2009 MODIS displacement measurements. The travel time of an ice particle under present-day flow conditions, i.e. a kind of relative age of ice within the Larsen C ice shelf is calculated using inverse streamlines going from the ice shelf edge toward the approximate inland boundary (not shown). The maximum travel time is ranging from 450 years to 550 years for the central areas of the ice shelf. The streamlines are also compared to the flowlines of the ice sheet (Fig. 10) to detect possible changes in the flow field. Computed streamlines and visible flowlines are mostly well aligned, confirming the high accuracy of the velocities matched, and implying at the same time that there has been no or little directional change in the ice-shelf flow over the last decades or few centuries. However, the four southernmost streamlines deviate significantly from the visible flowlines. It is unlikely that these deviations are due to matching errors of the velocity vectors because these four streamlines are interpolated from a number of independent velocity measurements. A possible explanation is thus that one or more of the glaciers Lewis Glacier, Ahlmann Glacier, Bills Gulch and Daspit Glacier have changed their discharge and thus diverted the ice flow from their neighbours.

5 Results for other ice shelves

In order to test the applicability and performance of the presented method for monitoring ice shelves dynamics in Antarctica in general, we also match other ice shelves. The objective of this study step is to indicate for what ice shelves or ice-shelf sections the method works and to characterize the necessary ground conditions. Larsen C exhibits comparably many flow features, which makes the matching successful. In addition, it is also comparably fast flowing, which favours detection of displacements at a statistically significant level. Other ice shelves may be more challenging in these respects.

Velocity fields for the ice shelves Ronne, Filchner, Riiser-Larsen, Fimbul, Amery, West, Shackleton, Ross and Getz are derived, and also the velocity field for Mertz Glacier. This is done for two different periods to also identify possible velocity changes. The images used are listed in Table 5. Velocity fields are shown in Fig. 11 and 12. Displacement matches are generated for the entire images shown, but non-significant displacements are removed to improve the readability and so are also clear mismatches

TCD
4, 31–75, 2010

as revealed by manual inspection. The parts of the ice shelves not covered by velocity arrows in the figures are hence not matched correctly or show no movement. Generally the method produces densely populated velocity fields for all ice shelves. Gaps in the velocity fields appear mostly where too few radiometric contrast features are present. This is evident for parts of the Fimbul (Fig. 11e), Getz (east) (Fig. 12a), Riiser-Larsen (Fig. 12c) and Shackleton (Fig. 12e) ice shelves. For Ross (east) (Fig. 11b) snow dunes seem to distract the matching and thus cause mismatches, and for Filchner (Fig. 11d) there are some clouds present in the images used. We also tried to match the Wilkins and Sulzberger ice shelves, but most parts of Wilkins had too little radiometric contrast and on Sulzberger most of the velocities were too small to be significant with the level of uncertainty given by the method and image type used.

For most of the ice shelves (Ross, Getz, Filchner, Riiser-Larsen and Amery) the maximum velocity measured was between 1000 and 1200 $\mathrm{m\,a^{-1}}$. Mertz and Ronne had somewhat higher maximum velocities with approximately 1400 $\mathrm{m\,a^{-1}}$ and Fimbul and West lower maximum velocities with 800 $\mathrm{m\,a^{-1}}$. The highest velocities were found at Shackleton ice shelf, where maximum velocity over the observational period was 1800 $\mathrm{m\,a^{-1}}$.

Three ice-shelf sections experienced small accelerations from the first period to the second period. A small glacier northwest of Ross ice shelf (Fig. 11a) had a mean speed increase of 34.8 $\mathrm{m\,a^{-1}}$. The uncertainty of this comparison is $\pm$32.4 $\mathrm{m\,a^{-1}}$. The ice to the west of the main ice stream of Shackleton ice shelf (Fig. 12e) increased in speed by 63.8 $\mathrm{m\,a^{-1}}$ with an uncertainty of $\pm$45.8 $\mathrm{m\,a^{-1}}$. Mertz Glacier speed (Fig. 12d) increased by 51.2 $\mathrm{m\,a^{-1}}$, with an uncertainty of $\pm$42.1 $\mathrm{m\,a^{-1}}$.

The western part of the West ice shelf (Fig. 12f) decelerated from the first period to the second. In the first period the mean speed was 762.1 $\mathrm{m\,a^{-1}}$ and in the second period the mean velocity for the same points was 570.7 $\mathrm{m\,a^{-1}}$. This corresponds to a deceleration of approximately 25%. The uncertainty of this comparison is 39.5 $\mathrm{m\,a^{-1}}$. Matching using NCC on the MODIS images and also manual inspection of Landsat and ASTER images confirmed the MODIS-derived deceleration.

6 Discussion

The comparison between MODIS and Landsat derived velocities reveals that MODIS derived velocities are accurate enough to derive velocities for ice shelves, even for a few years of separation between the images. These velocities can also be used to study dynamic changes with satisfying accuracy. This is possible, in spite of the large pixel size of 250×250 m, because the accuracy of the measurements is approximately 1/4 pixel using orientation correlation.

Both clouds, surface changes and lack of contrast can hinder successful matching. For the MODIS matching on Larsen C in the first period 2002–2006 it is mostly surface change between the two image acquisitions that hinders successful matching, but also lack of radiometric contrast. For the MODIS matching in the second period 2006–2009, the areas that are not correctly matched are mostly obscured by clouds. Successful matching of Landsat images is mainly hindered by the lack of radiometric contrast.

Average difference and RMS between the results when summing up the MODIS measurements from 2002–2006 and 2006–2009, and comparing them to the MODIS measurements directly for 2002–2009, are larger over the ice shelf and smaller over stable ground. The most important reason for this is that the velocity measurements are repeated on points with fixed geolocation, i.e. points that do not follow the ice movement. Thus, strain happening as the ice moves toward the ice shelf front is not accounted for. Another reason for the larger difference on the ice shelf is that it is easier to identify erroneous matches over stable ground than over the moving ice. It is more difficult to exclude mismatches from a nominally varying velocity field (ice shelf) than from a nominally constant one (stable ground). This is especially a problem where there are few measurements in close vicinity, which is the case for matching of the 2002 and 2009 images.

Matching windows have to be chosen to be considerably larger (in pixels) for the Landsat images compared to the MODIS images in order to obtain successful matches. The main reason for that is due to the typical (low) density of contrast features on

Larsen C such as crevasses. In the case of window sizes smaller than this density, most moving window positions simply contain not enough radiometric contrast to enable successful matching. In addition, the Landsat data have to be filtered to remove high frequencies, because the Landsat 7 ETM+ pan images contain detector noise of several digital numbers (DN), much more than the MODIS data, as can easily be explored over the vast low-contrast areas on the images. This high noise level within the 15 m ETM+ pan data compared to the 250 m MODIS data is a direct consequence of the much smaller instantaneous field of view and related weaker SNR in the detector. The high noise level in the ETM+ pan data requires relatively larger matching window sizes. It will be interesting to test how the potential gain in matching performance from using less noisy 30 m multispectral ETM+ or TM data relates to the potential loss in matching performance due to the reduced spatial resolution of 30 m in contrast to 15 m.

Subpixel accuracy relative to pixel size is poorer for the Landsat 7 ETM+ pan images compared to the MODIS images. This is mainly because the subpixel accuracy of the Landsat sensor is poorer, and because of the above sensor noise, which requires low-pass filtering. Low-pass filtered images give a less pronounced correlation peak, which has then to be used to derive subpixel accuracy.

OC is better suited for image matching in this particular study. OC produces more correct matches than NCC for the MODIS images. It is capable of matching Landsat images that have regular data voids after the failure of the SLC in 2003. OC is also faster than NCC. The clearest advantage of NCC against OC is that the size of the matching windows can be smaller, and thus more independent, i.e. not overlapping displacements can be measured. However, reduced window size leads, in turn, to reduced accuracy. When matching low resolution images the best possible accuracy is needed in order to obtain meaningful results. In other studies where better spatial resolution of the velocity field is needed over best possible accuracy, NCC can be a better choice.

Images with 12 bit radiometric resolution are better suited for image matching in this area than images with 8 bit radiometric resolution because they produce more correct matches using both OC and NCC. It is therefore possible that areas that give no correct matches using 8 bit images can give correct matches if 12 bit images are used instead. However, 8 bit images give correct matches in most of the areas, and unless measurements over a relatively featureless area are needed, they produce satisfying results. Some points are even matched with the 8 bit images that are not matched with the 12 bit images. These can be mismatches that are not revealed by our selection procedure. However, the reduced noise level in 8 bit images compared to 12 bit images from the same sensor will also lead to more robust matches in 8 bit data. In the figures, there seems to be a difference in the effect of using 12 bit images instead of 8 bit images between OC and NCC. However, this is just an apparent, not a real difference because NCC is matched on manually selected points in high-contrast areas. NCC matching in a regular grid with large window sizes gives too few matches for the MODIS images applied in our study.

It is possible that creating a 12 bit radiometric resolution image from the original 2002 MODIS data would have increased the number of MODIS matches in the first period due to more contrast. However, since the difference between 12 bit and 8 bit resolution turned out to be small, this is not done.

Aligning images before the matching procedure improves the results, both when it comes to the accuracy of the measurements and the number of correct measurements. This is particularly important for the Landsat images which only have an absolute accuracy of 250 m, or 16.7 pixels (NASA, 1996). In order to get more correct matches on the ice shelf, the images were sometimes also aligned locally based on an assumed first-order displacement or a first matching iteration.

The presented method works well on most parts of the ice shelves investigated. The main factor that hinders successful matching during cloud-free conditions is the lack of radiometric contrast features, mostly flow features. Also snow dunes can be a problem when they cover the flow features in one of the images. Because of the uncertainty of the displacement measurements, some ice shelves actually showed velocities below

TCD
4, 31–75, 2010

the significance level.

Both Skvarca (1994) and Glasser et al. (2009) have conducted velocity measurements on Larsen C. Skvarca (1994) found that the heavily crevassed area just north of Kenyon Peninsula (see Fig. 1 for location) moved with velocities ranging from 430 to 550 m a^{-1} between 1975 and 1986, the velocities increasing as the ice moved seawards. In the same area we find velocities ranging from 410 to 630 m a^{-1}. Our results are therefore consistent with previous results in this area. Glasser et al. (2009) measured the velocities between 2002 and 2007 in a crevassed area close to the ice shelf edge in the middle of the ice shelf by an unspecified method. They measured a mean velocity of 640 m a^{-1} in this area. We measure velocities of 670 m a^{-1}, which is also consistent with their measurements in this area.

The acceleration that is observed at Larsen B and at one section in the north of Larsen C can be put in context with the elevation decrease that Shepherd et al. (2003) measured between 1992 and 2001. The acceleration is found in the areas where also the largest elevation decrease was found. It is therefore likely that the acceleration can be attributed to the reduced backstress that a thinning ice shelf causes. This has been observed earlier for tidewater glaciers on the Antarctic Peninsula (Pritchard and Vaughan, 2007). However Glasser et al. (2009), who studied the surface structure of the Larsen C ice shelf from features such as crevasses and flowlines, did not see any large changes in the surface structure of the ice shelf between 1963 and 2007, and concluded that the ice shelf is stable. It is therefore likely that the acceleration seen so far is too small to have an impact on the visible surface structures.

The most likely explanation for the deceleration of the West ice shelf is that the ice shelf is already detached from its contributing glaciers. The satellite images support this hypothesis because there is a intersection going across the flow direction in the inner part of the ice shelf where there are no flow features. However, the detached part is probably still grounded and therefore not an iceberg.

7 Conclusions and outlook

We have demonstrated that repeat optical MODIS satellite images are well suited for measuring and monitoring velocities on Antarctic ice shelves in spite of their low spatial resolution of 250 m. This is done by comparing velocities derived from MODIS images over the Larsen C ice shelf with velocities derived from Landsat 7 ETM+ pan images with a spatial resolution of 15 m. The results agree well. For the period 2002–2006 the difference between MODIS and Landsat derived velocities are $-15.4\,\mathrm{m\,a^{-1}}$ and $13.0\,\mathrm{m\,a^{-1}}$ for two sections on the ice shelf, and for the period 2006–2009 it is $-26.7\,\mathrm{m\,a^{-1}}$ and $27.9\,\mathrm{m\,a^{-1}}$ for the same sections. The uncertainties of the method are $\pm 18.3\,\mathrm{m\,a^{-1}}$ and $\pm 19.1\,\mathrm{m\,a^{-1}}$ for the first period, and $\pm 22.4\,\mathrm{m\,a^{-1}}$ and $\pm 22.4\,\mathrm{m\,a^{-1}}$ for the second period. Uncertainties are calculated as the RSS of the RMS of the displacement measurements over stable ground and the image-to-image registration accuracy from the literature.

It is possible to obtain better results from matching MODIS images than obtained here. In this study we chose MODIS images with small amount of clouds acquired as close as possible in time to the Landsat images. Images with less clouds and of better radiometric quality were available, but then the time separation between the MODIS and the Landsat images would have been larger. Short time separation was considered to be more important than maximizing the number of matches for this validation study.

Both OC operating in the frequency domain and NCC operating in the spatial domain are tested for matching the images. OC is faster, gives more correct matches, and can match images with regular noise because it is not sensitive to information restricted to few frequencies. The latter makes it possible to match Landsat 7 images with striped data voids after the failure of the SLC. NCC can match images with smaller matching window sizes than OC. However, this reduces the accuracy of the measurements. In situations where small window sizes are important, for example where the velocity varies over short distances, NCC can produce a higher resolution velocity field, but the accuracy will then be reduced. In this study both accuracy, number of correct matches and insensitivity to information constrained to few frequencies were important. Therefore OC produced the best results both for MODIS and Landsat images. In total, we achieved a sub-pixel accuracy of about 1/4 of a pixel for matching displacements based on repeat MODIS data.

The remains of Larsen B and one section in the north of Larsen C accelerated from the 2002–2006 period to the 2006–2009 period. These areas also thinned between 1992 and 2001 (Shepherd et al., 2003), which can have reduced the backstress and thereby caused the acceleration. However, these changes have so far not changed the surface structure of the ice shelf in a visually obvious way (Glasser et al., 2009).

From a deviation between calculated streamlines and flowlines visible in the MODIS images of Larsen C we find that there is a possible change in discharge from one or more of the glaciers Lewis Glacier, Ahlmann Glacier, Bills Gulch and Daspit Glacier. The same streamlines indicate a travel time of the ice of the Larsen C ice shelf between the inland boundary and the ice edge of up to about 450 to 550 years. We applied our method successfully to ten other ice shelves around Antarctica and present an initial selection of ice shelves that could be monitored that way, confirming that the method developed here is, indeed, capable for Antarctic ice shelf velocity monitoring in general.

Our study opens for a new strategy that complements existing approaches, mainly based on SAR interferometry and tracking, to monitor and better understand dynamics, calving rates and stability of ice shelves around Antarctica. In addition to the MODIS data tested here, other low-resolution, but large coverage and high repeat-rate sensors such as ESA's Envisat MERIS are available for this purpose.

Acknowledgements. MODIS data are courtesy of NASA, and were prepocessed and obtained from NSIDC through http://www.nsidc.org. Landsat data are courtesy of USGS and were obtained through http://glovis.usgs.gov. We are grateful to these institutions for making their unique data available. This study is funded by The Research Council of Norway (NFR) through the CORRIA project (no. 185906/V30) and serves in addition as test study for the ESA DUE GlobGlacier project and the NFR IPY Glaciodyn project.

References

Argyriou, V. and Vlachos, T.: Quad-tree motion estimation in the frequency domain using gradient correlation, IEEE Transactions On Multimedia, 9, 1147–1154, 2007. 40

Berthier, E., Vadon, H., Baratoux, D., Arnaud, Y., Vincent, C., Feigl, K., Remy, F., and Legresy, B.: Surface motion of mountain glaciers derived from satellite optical imagery, Remote Sens. Environ., 95, 14–28, doi:10.1016/j.rse.2004.11.005, 2005. 33

Bindschadler, R. A., Fahnestock, M. A., Skvarca, P., and Scambos, T. A.: Surface-velocity field of the northern Larsen Ice Shelf, Antarctica, Ann. Glaciol., 20, 319–326, 1994. 33, 35

Brown, L. G.: A survey of image registration techniques, Comput. Surv., 24, 325–376, 1992. 33

Cook, A. J. and Vaughan, D. G.: Overview of areal changes of the ice shelves on the Antarctic Peninsula over the past 50 years, The Cryosphere Discuss., 3, 579–630, 2009, http://www.the-cryosphere.net/3/579/2009/. 35

De Angelis, H. and Skvarca, P.: Glacier surge after ice shelf collapse, Science, 299, 1560–1562, 2003. 35

Debella-Gilo, M. and Kääb, A.: Sub-pixel precision algorithms for normalized cross-correlation based image matching of mass movements, in preparation, 2010. 38

Fitch, A. J., Kadyrov, A., Christmas, W. J., and Kittler, J.: Orientation Correlation, in: British Machine Vision Conference, 133–142, 2002. 38

Glasser, N. F., Kulessa, B., Luckman, A., Jansen, D., King, E. C., Sammonds, P. R., Scambos, T. A., and Jezek, K. C.: Surface structure and stability of the Larsen C ice shelf, Antarctic Peninsula, J. Glaciol., 55, 400–410, 2009. 33, 52, 54

Griggs, J. A. and Bamber, J. L.: Ice shelf thickness over Larsen C, Antarctica, derived from satellite altimetry, Geophys. Res. Lett., 36, L19501, doi:10.1029/2009GL039527, 2009. 36

Kaufmann, V. and Ladstädter, R.: Quantitative analysis of rock glacier creep by means of digital photogrammetry using multitemporal aerial photographs: two case studies in the Austrian Alps, Proceedings of the 8th International Conference on Permafrost, 525–530, 2003. 38

Kääb, A.: Monitoring high-mountain terrain deformation from repeated air- and spaceborne optical data: examples using digital aerial imagery and ASTER data, ISPRS Journal of Photogrammetry and Remote Sensing, 57, 39–52, 2002. 33, 38

Kääb, A.: Combination of SRTM3 and repeat ASTER data for deriving alpine glacier flow velocities in the Bhutan Himalaya, Remote Sens. Environ., 94, 463–474, doi:10.1016/j.rse.2004.

11.003, 2005. 33, 38
Kääb, A., Gudmundsson, G. H., and Hoelzle, M.: Surface deformation of creeping mountain permafrost. Photogrammetric investigations on Rock Glacier Murtèl, Swiss Alps, Proceedings of the 7th International Conference on Permafrost, 531–537, 1998. 46
Kääb, A., Lefauconnier, B., and Melvold, K.: Flow field of Kronebreen, Svalbard, using repeated Landsat 7 and ASTER data, Ann. Glaciol. 42, 7–13, 2005. 33
MacAyeal, D. R., Scambos, T. A., Hulbe, C. L., and Fahnestock, M. A.: Catastrophic ice-shelf break-up by an ice-shelf-fragment-capsize mechanism, J. Glaciol., 49, 22–36, 2003. 36
Meredith, M. P. and King, J. C.: Rapid climate change in the ocean west of the Antarctic Peninsula during the second half of the 20th century, Geophys. Res. Lett., 32, L19604, doi: 10.1029/2005GL024042, 2005. 35
NASA, G.: Landsat 7 System Specification, NASA Goddard Space Flight Center, 1996. 42, 51
Pritchard, H. D. and Vaughan, D. G.: Widespread acceleration of tidewater glaciers on the Antarctic Peninsula, J. Geophys. Res., 112, F03S29, doi:10.1029/2006JF000597, 2007. 35, 52
Quincey, D. J. and Glasser, N. F.: Morphological and ice-dynamical changes on the Tasman Glacier, New Zealand, 1990–2007, Global and Planetary Change, 68, 185–197, doi:10.1016/j.gloplacha.2009.05.003, 2009. 33
Rack, W. and Rott, H.: Pattern of retreat and disintegration of the Larsen B ice shelf, Antarctic Peninsula, Ann. Glaciol., 39, 505–510, 2004. 35
Rignot, E., Casassa, G., Gogineni, P., Krabill, W., Rivera, A., and Thomas, R.: Accelerated ice discharge from the Antarctic Peninsula following the collapse of Larsen B ice shelf, Geophys. Res. Lett., 31, L18401, doi:10.1029/2004GL020697, 2004. 35
Rignot, E., Casassa, G., Gogineni, S., Kanagaratnam, P., Krabill, W., Pritchard, H., Rivera, A., Thomas, R., Turner, J., and Vaughan, D.: Recent ice loss from the Fleming and other glaciers, Wordie Bay, West Antarctic Peninsula, Geophys. Res. Lett., 32, L07502, doi:10.1029/2004GL021947, 2005. 35
Rignot, E., Bamber, J. L., Van Den Broeke, M. R., Davis, C., Li, Y., Van De Berg, W. J., and Van Meijgaard, E.: Recent Antarctic ice mass loss from radar interferometry and regional climate modelling, Nature Geosci., 1, 106–110, doi:10.1038/ngeo102, 2008. 35
Rolstad, C., Amlien, J., Hagen, J. O., and Lunden, B.: Visible and near-infrared digital images for determination of ice velocities and surface elevation during a surge on Osbornebreen, a tidewater glacier in Svalbard, Ann. Glaciol., 24, 255–261, 1997. 33

Rott, H., Skvarca, P., and Nagler, T.: Rapid collapse of northern Larsen Ice Shelf, Antarctica, Science, 271, 788–792, 1996. 35

Scambos, T. and Bohlander, J.: Glaciers of Larsen B embayment area show marked speed-up since shelf collapse, Eos Trans. AGU, 86, Fall Meet. Suppl., C11C–0829, 2003. 35

Scambos, T., Ross, R., Bauer, R., Yermolin, Y., Skvarca, P., Long, D., Bohlander, J., and Haran, T.: Calving and ice-shelf break-up processes investigated by proxy: Antarctic tabular iceberg evolution during northward drift, J. Glaciol., 54, 579–591, 2008. 36

Scambos, T., Bohlander, J., and Raup, B.: "Images of Antarctic ice shelves", National Snow and Ice Data Center, online available at: http://nsidc.org/data/iceshelves_images/, 2009. 37, 64, 66, 74, 75

Scambos, T. A., Hulbe, C., Fahnestock, M., and Bohlander, J.: The link between climate warming and break-up of ice shelves in the Antarctic Peninsula, J. Glaciol., 46, 516–530, 2000. 36

Scambos, T. A., Bohlander, J. A., Shuman, C. A., and Skvarca, P.: Glacier acceleration and thinning after ice shelf collapse in the Larsen B embayment, Antarctica, Geophys. Res. Lett., 31, L18402, doi:10.1029/2004GL020670, 2004. 35

Scambos, T. A., Dutkiewicz, M. J., Wilson, J. C., and Bindschadler, R. A.: Application of image cross-correlation to the measurement of glacier velocity using satellite image data, Remote Sens. Environ., 42, 177–186, 1992. 33

Scherler, D., Leprince, S., and Strecker, M. R.: Glacier-surface velocities in alpine terrain from optical satellite imagery - Accuracy improvement and quality assessment, Remote Sens. Environ., 112, 3806–3819, 2008. 33

Shepherd, A., Wingham, D., Payne, T., and Skvarca, P.: Larsen ice shelf has progressively thinned, Science, 302, 856–859, 2003. 36, 52, 54

Skvarca, P.: Fast recession of the northern Larsen Ice Shelf monitored by space images, Ann. Glaciol., 17, 317–321, 1993. 35

Skvarca, P.: Changes and surface features of the Larsen Ice Shelf, Antarctica, derived from Landsat and Kosmos mosaics, Ann. Glaciol., 20, 6–12, 1994. 33, 52

Skvarca, P., Rack, W., and Rott, H.: 34 year satellite time series to monitor characteristics, extent and dynamics of Larsen B Ice Shelf, Antarctic Peninsula, Ann. Glaciol., 29, 255–260, 1999. 36

Skvarca, P., Raup, B., and De Angelis, H.: Recent behaviour of Glaciar Upsala, a fast-flowing calving glacier in Lago Argentino, southern Patagonia, Ann. Glaciol., 36, 184–188, 2003. 33

Skvarca, P., De Angelis, H., and Zakrajsek, A.: Climatic conditions, mass balance and dynamics of Larsen B ice shelf, Antarctic Peninsula, prior to collapse, Ann. Glaciol., 39, 557–562, 2004. 36

Turner, J., Colwell, S. R., Marshall, G. J., Lachlan-Cope, T. A., Carleton, A. M., Jones, P. D., Lagun, V., Reid, P. A., and Iagovkina, S.: Antarctic climate change during the last 50 years, Int. J. Climatol., 25, 279–294, 2005. 35

Vieli, A., Payne, A. J., Du, Z. J., and Shepherd, A.: Numerical modelling and data assimilation of the Larsen B ice shelf, Antarctic Peninsula, Philos. T. Roy. Soc. A, 364, 1815–1839, 2006. 36

Wolfe, R., Nishihama, M., Fleig, A., Kuyper, J., Roy, D., Storey, J., and Patt, F.: Achieving sub-pixel geolocation accuracy in support of MODIS land science, Remote Sens. Environ., 83, 31–49, 2002. 42

Zitova, B. and Flusser, J.: Image registration methods: a survey, Image and Vision Computing, 21, 977–1000, 2003. 33

Table 1. MODIS and Landsat satellite images used for the velocity measurements.

Larsen C South		Larsen C North	
MODIS	Landsat	MODIS	Landsat
17 Mar 2002	22 Nov 2001	17 Mar 2002	15 Apr 2002
5 Jan 2006	4 Jan 2006	5 Jan 2006	4 Jan 2006
1 Jan 2009	12 Jan 2009	28 Nov 2008	11 Dec 2008

Table 2. Root mean square error (RMS) of displacement measurements obtained using frequency domain matching over stable ground. The number of measurements is indicated by *n*.

Image pair	RMS_x m	RMS_y m	*n*
MODIS 2002–2006	28.0	38.7	106
MODIS 2006–2008	24.2	26.0	188
MODIS 2006–2009	21.2	35.9	176
MODIS 2002–2009	30.0	36.1	183
Landsat 2001–2006 South	4.72	8.00	71
Landsat 2006–2009 South	7.75	10.6	47
Landsat 2002–2006 North	–	–	–
Landsat 2006–2008 North	–	–	–

Table 3. Average velocity and acceleration measured from MODIS and Landsat images for 6 points in the Larsen C North section and 28 points in the Larsen C South section. The RMS of the average is also given.

	Average velocity 1. period south $m\,a^{-1}$	Average velocity 2. period south $m\,a^{-1}$	Average acceleration 2. period–1. period south $m\,a^{-1}$	Average velocity 1. period north $m\,a^{-1}$	Average velocity 2. period north $m\,a^{-1}$	Average acceleration 2. period–1. period north $m\,a^{-1}$
MODIS	430.2 ± 177.9	427.1 ± 172.5	−3.1 ± 38.0	383.7 ± 22.9	425.8 ± 39.1	42.0 ± 21.3
Landsat	445.6 ± 157.4	453.8 ± 159.6	8.2 ± 20.9	370.8 ± 20.1	397.9 ± 30.0	27.1 ± 14.5
MODIS – Landsat	−15.4 ± 39.6	−26.7 ± 40.1	−11.3 ± 44.4	13.0 ± 20.5	27.9 ± 33.5	14.9 ± 22.7

Table 4. Uncertainty of the measured MODIS and Landsat displacements and accelerations. The root sum square (RSS) of the uncertainties are also given and can be compared with the deviations given in the lower row of Table 3.

	Uncertainty 1. period south $m\,a^{-1}$	Uncertainty 2. period south $m\,a^{-1}$	Uncertainty 2. period–1. period south $m\,a^{-1}$	Uncertainty 1. period north $m\,a^{-1}$	Uncertainty 2. period north $m\,a^{-1}$	Uncertainty 2. period–1. period north $m\,a^{-1}$
MODIS	± 18.1	± 21.8	± 28.3	± 18.1	± 21.1	± 27.8
Landsat	± 2.86	± 4.96	± 5.73	± 6.01	± 7.63	± 9.71
RSS	± 18.3	± 22.4	± 28.9	± 19.1	± 22.4	± 29.4

Table 5. MODIS images used for deriving velocities and velocity changes for ten other ice shelves in Antarctica.

Ice shelf	Time 1	Time 2	Time 3
Ross West	28 Dec 2001	5 Dec 2005	8 Dec 2008
Ross East	6 Oct 2002	25 Oct 2005	27 Dec 2008
Getz	21 Jan 2003	1 Mar 2006	11 Feb 2009
Ronne	3 Dec 2002	4 Oct 2006	13 Oct 2008
Filchner	3 Dec 2002	23 Feb 2006	9 Mar 2009
Riiser-Larsen	19 Feb 2003	29 Jan 2006	14 Feb 2009
Fimbul	2 Mar 2003	1 Mar 2006	11 Mar 2009
Amery	20 Feb 2002	3 Mar 2006	19 Feb 2009
West	20 Jan 2003	16 Mar 2006	19 Mar 2009
Shackleton	26 Feb 2003	20 Feb 2006	23 Feb 2009
Mertz	15 Mar 2002	11 Mar 2006	2 Mar 2009

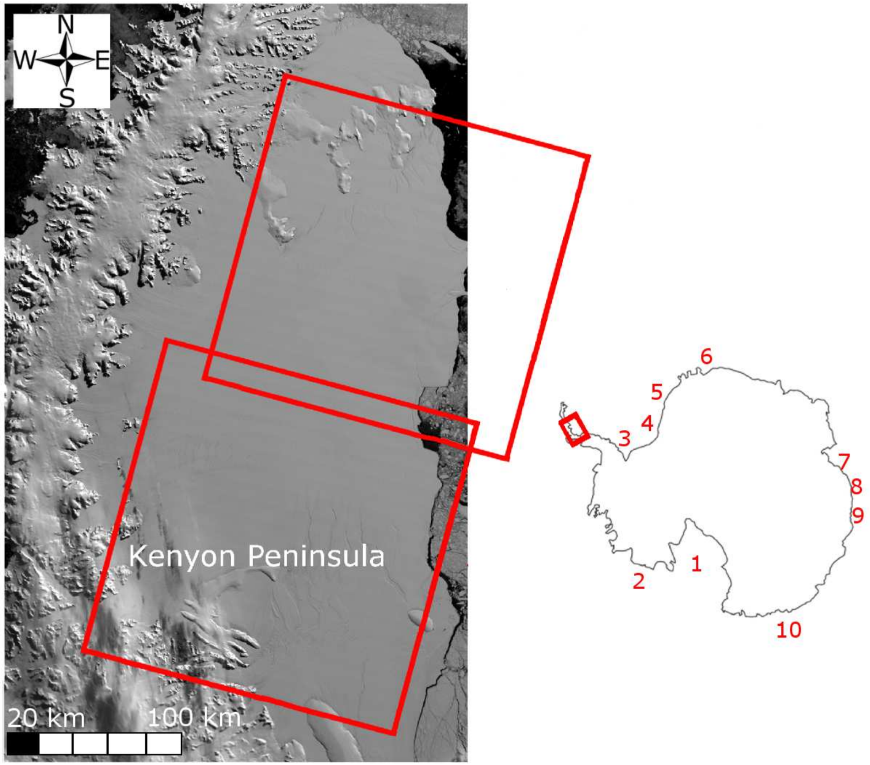

Fig. 1. Sketch map over Antarctica (right) and image of Larsen C ice shelf (left). The position of the MODIS image is indicated as red rectangle in the right panel and it forms the background in the left panel. The position of the Landsat validation images are indicated in red in the left panel. The numbers mark the locations of the other ice shelves investigated: 1. Ross, 2. Getz east, 3. Ronne, 4. Filchner, 5. Riiser-Larsen, 6. Fimbul, 7. Amery, 8. West, 9. Shackleton, 10. Mertz glacier. The MODIS image is from 2002 and was preprocessed by Scambos et al. (2009).

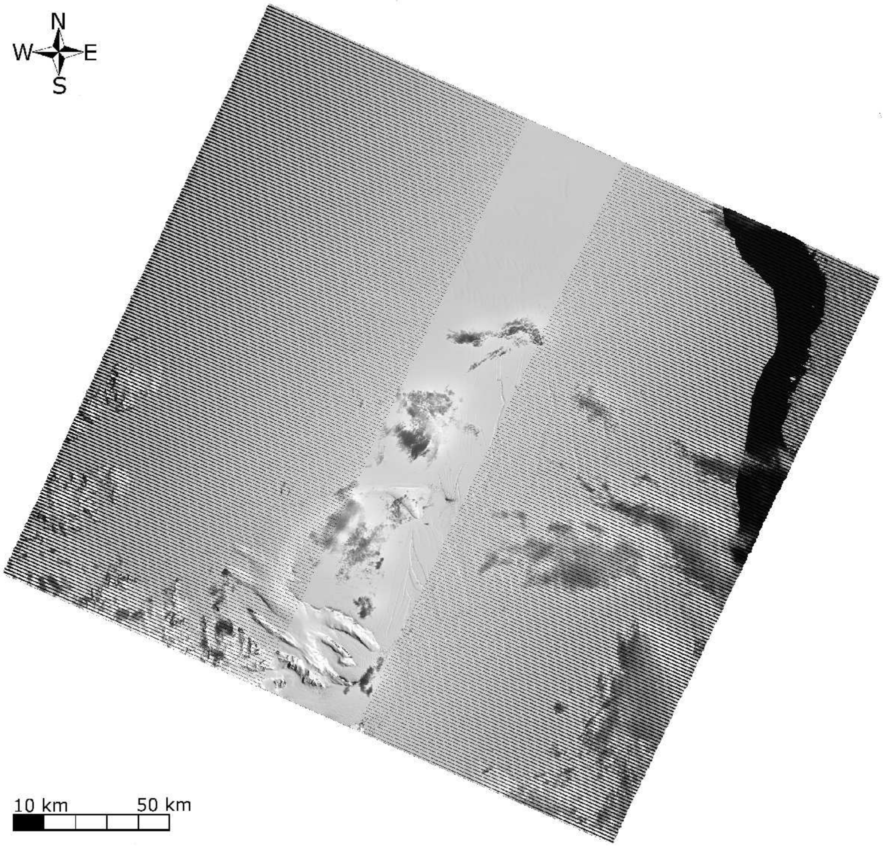

Fig. 2. Landsat 7 ETM+ pan image from 2006 used in this study that shows the regular cross-track data voids caused by the failure of the Scan Line Corrector.

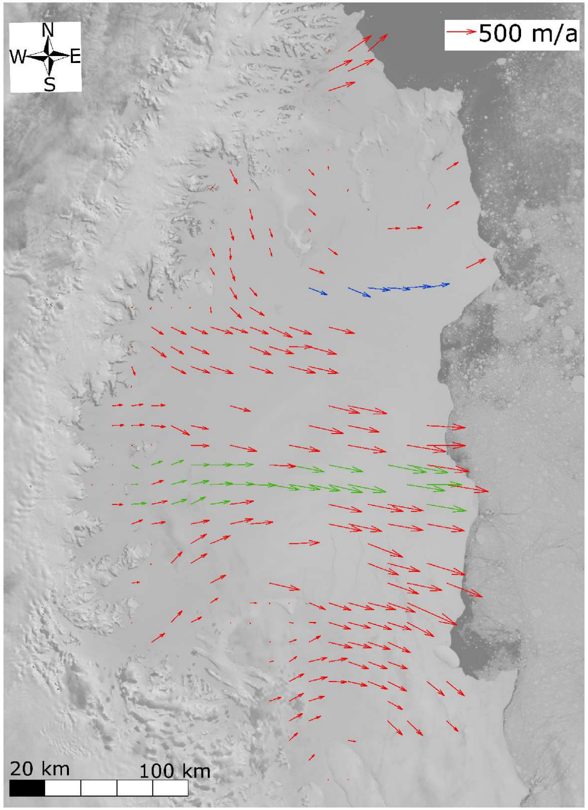

Fig. 3. Average annual velocity between 2002 and 2006 measured with orientation correlation on MODIS images. Blue and green colors indicate that these measurements are compared with Landsat measurements. The underlying MODIS image of 2009 is preprocessed by Scambos et al. (2009).

TCD
4, 31–75, 2010

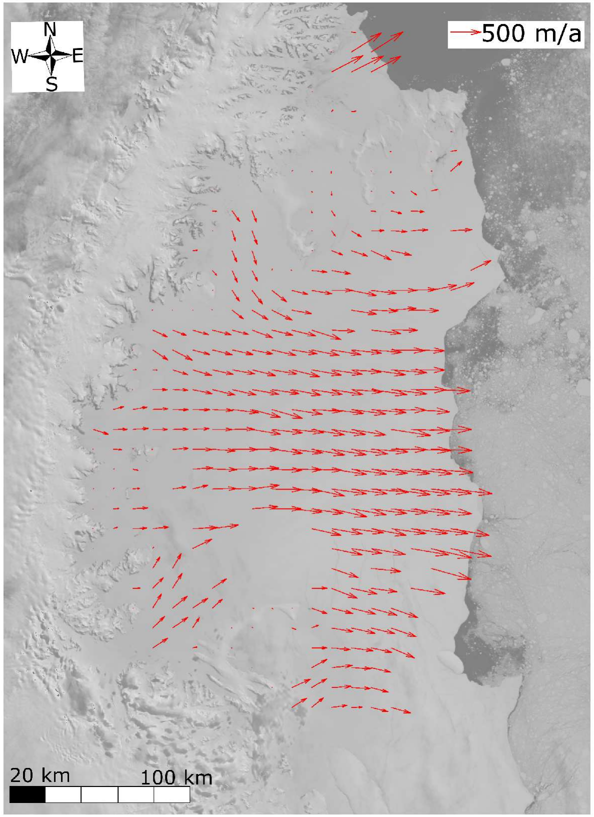

Fig. 4. Average annual velocity between 2006 and 2009 measured with orientation correlation on MODIS images.

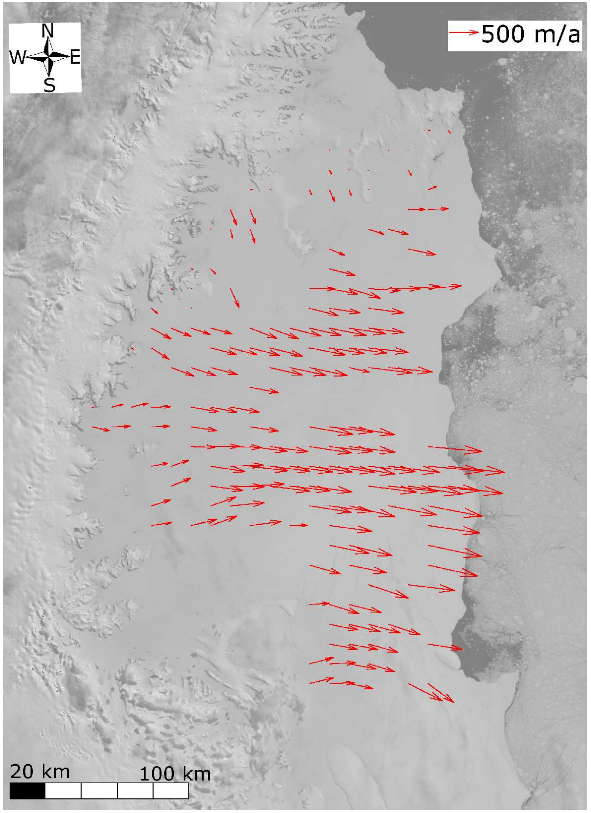

Fig. 5. Average annual velocity between 2002 and 2009 measured with orientation correlation on MODIS images.

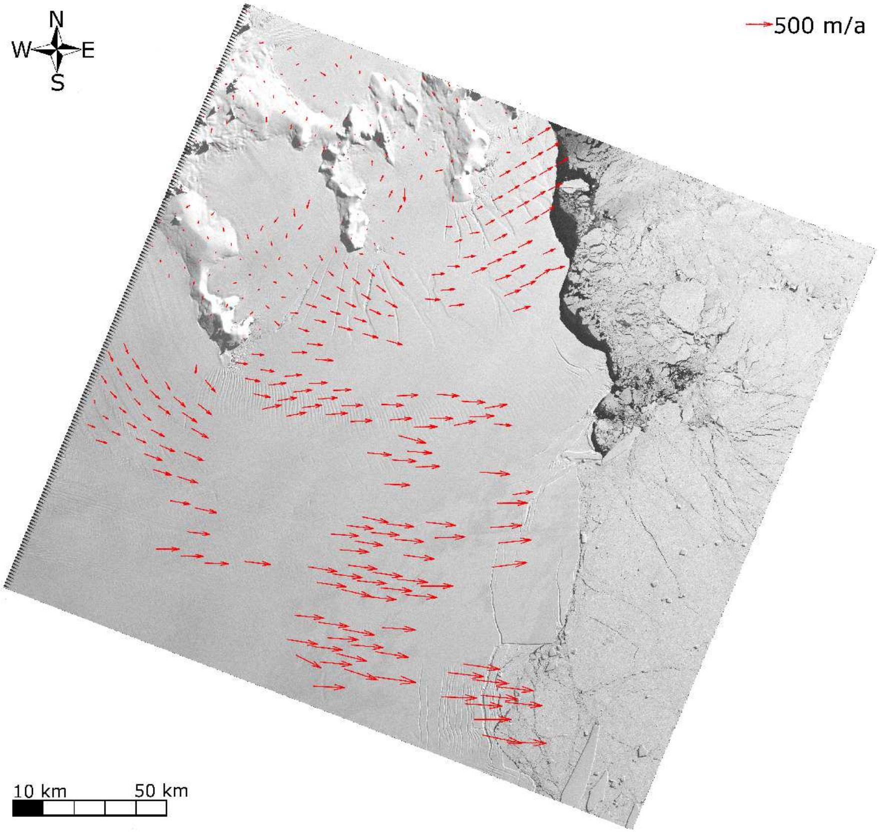

Fig. 6. Average annual velocity between 2006 and 2008 measured with orientation correlation on Landsat 7 ETM+ pan images over Larsen C North. Underlying Landsat image of 2002.

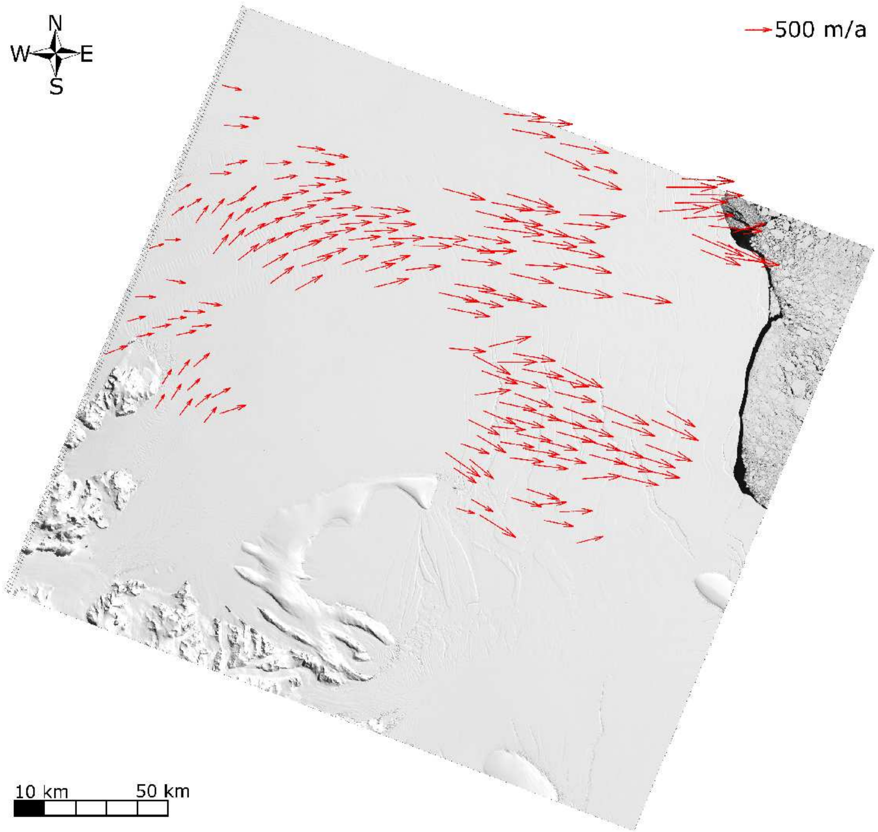

Fig. 7. Average annual velocity between 2006 and 2009 measured with orientation correlation on Landsat 7 ETM+ pan images over Larsen C South. Underlying Landsat image of 2002.

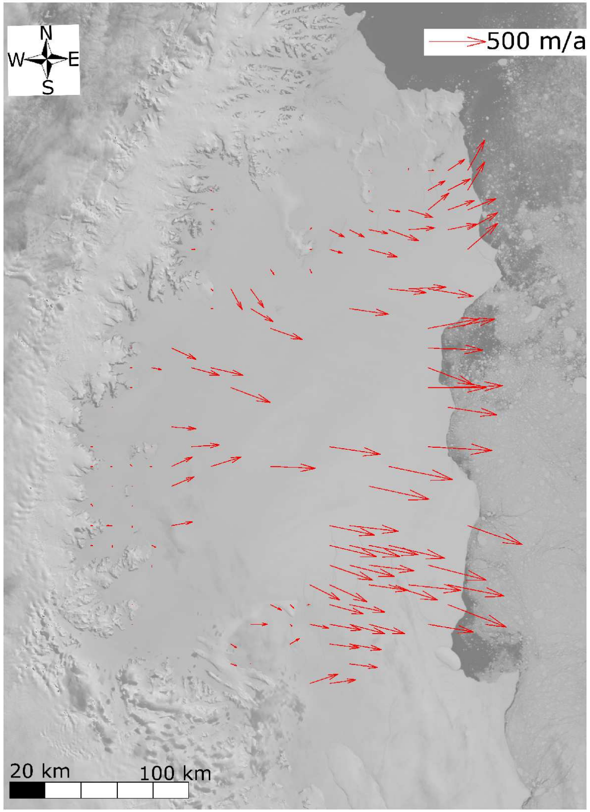

Fig. 8. Average annual velocity between 2006 and 2009 measured with normalized cross-correlation using a window size of 44×44 pixels (the same as used for the orientation correlation) on MODIS images.

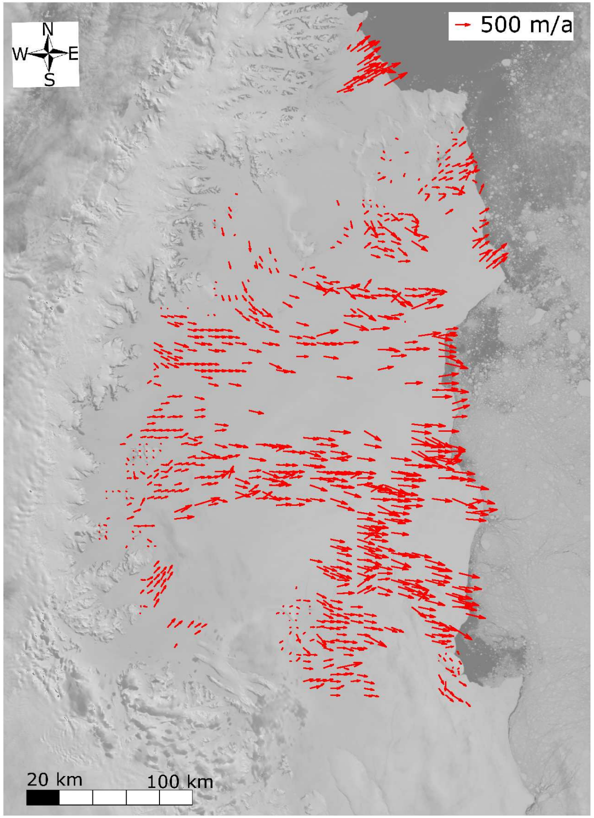

Fig. 9. Average annual velocity between 2006 and 2009 measured with normalized cross-correlation using a window size of 15×15 pixels on MODIS images.

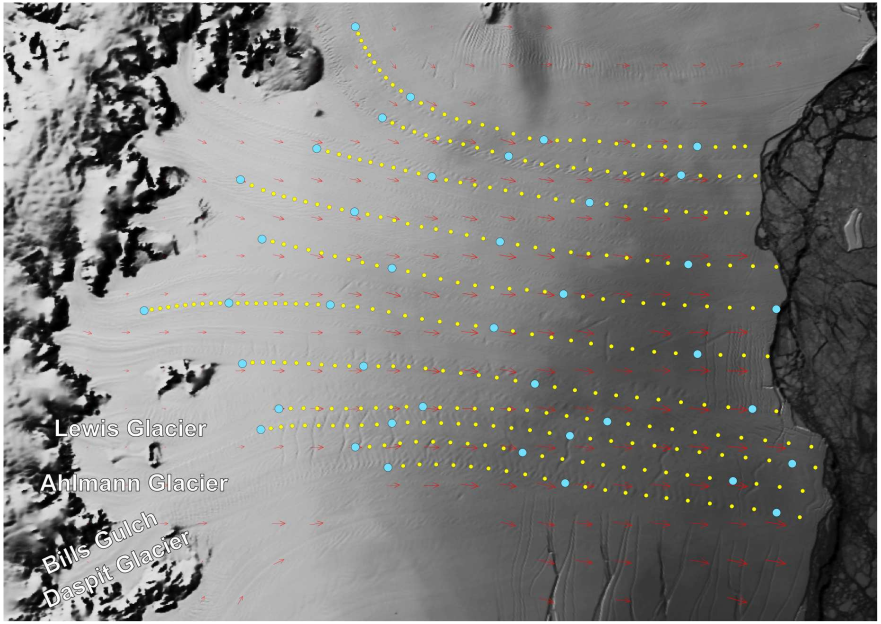

Fig. 10. Streamlines calculated from the 2006–2009 displacement measurements. Yellow dots are separated by 10 years of displacement and blue dots by 100 years of displacement. Underlying MODIS image is from 2008.

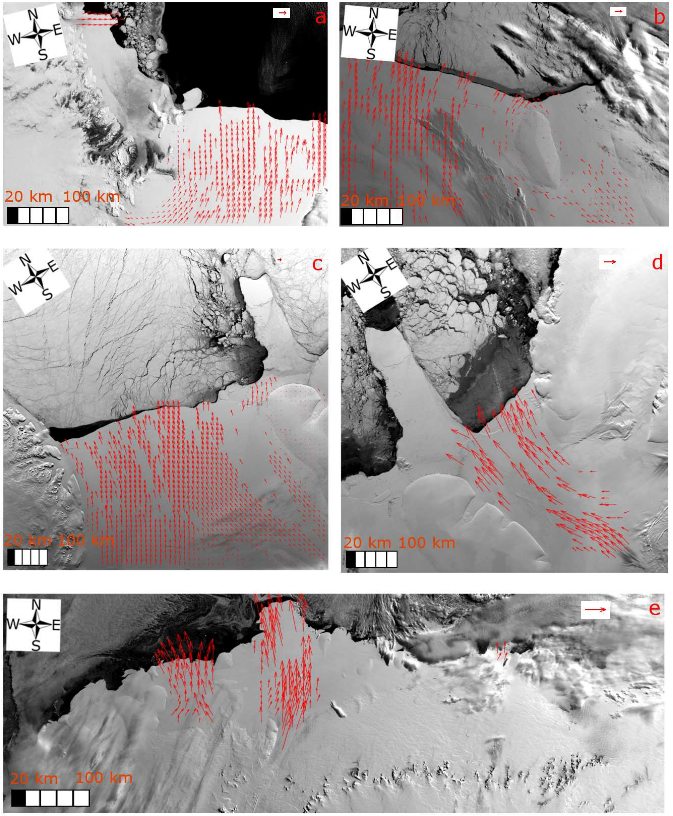

Fig. 11. The velocity fields of nine ice shelves and one glacier in Antarctica derived from repeat MODIS images using orientation correlation. **(a)** Ross (west),**(b)** Ross (east), **(c)** Ronne, **(d)** Filchner, **(e)** Fimbul. The arrow in the upper left corner indicate a velocity of 500 m a^{-1}. The underlying images are preprocessed by Scambos et al. (2009).

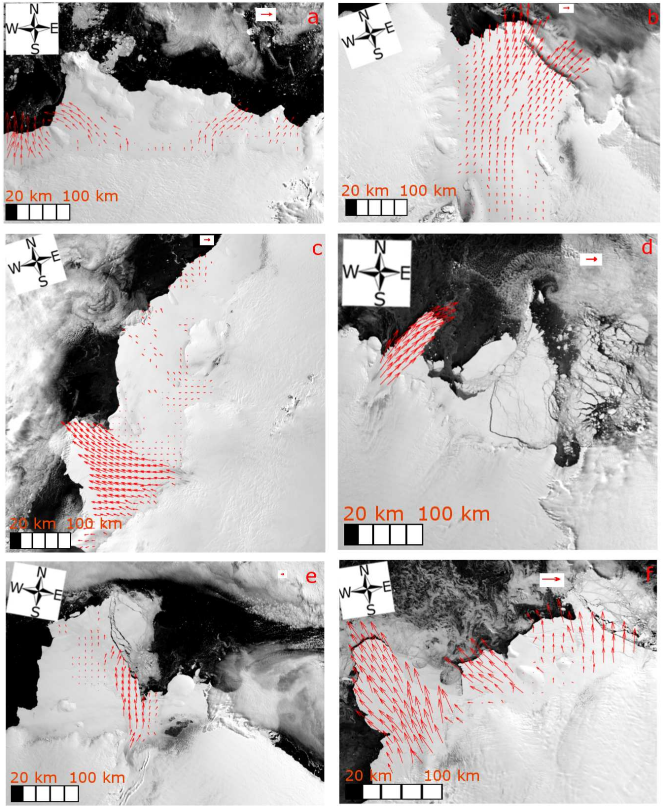

Fig. 12. The velocity fields of nine ice shelves and one glacier in Antarctica derived from repeat MODIS images using orientation correlation. **(a)** Getz (east), **(b)** Amery, **(c)** Riiser-Larsen, **(d)** Mertz, **(e)** Shackleton, **(f)** West. The arrow in the upper left corner indicate a velocity of 500 m a^{-1}. The underlying images are preprocessed by Scambos et al. (2009).